On the Extratropical Influence of Variations of the Upper-Tropospheric Equatorial Zonal-Mean Zonal Wind during Boreal Winter

GEREON GOLLAN AND RICHARD J. GREATBATCH

GEOMAR Helmholtz Centre for Ocean Research Kiel, Kiel, Germany

(Manuscript received 6 March 2014, in final form 25 September 2014)

ABSTRACT

Variations in the global tropospheric zonal-mean zonal wind [U] during boreal winter are investigated using rotated empirical orthogonal functions applied to monthly means. The first two modes correspond to the northern and southern annular mode and modes 3 and 4 represent variability in the tropics. One is related to El Niño–Southern Oscillation and the other has variability that is highly correlated with the time series of [U] at 150 hPa between 5°N and 5°S $[U150]_E$ and is related to activity of the Madden–Julian oscillation. The extratropical response to $[U150]_E$ is investigated using linear regressions of 500-hPa geopotential height onto the $[U150]_E$ time series. Use is made of reanalysis data and of the ensemble mean output from a relaxation experiment using the European Centre for Medium-Range Weather Forecasts model in which the tropical atmosphere is relaxed toward reanalysis data. The regression analysis reveals that a shift of the Aleutian low and a wave train across the North Atlantic are associated with $[U150]_E$. It is found that the subtropical waveguides and the link between the North Pacific and North Atlantic are stronger during the easterly phase of $[U150]_E$. The wave train over the North Atlantic is associated with Rossby wave sources over the subtropical North Pacific and North America. Finally, it is shown that a linear combination of both $[U150]_E$ and the quasi-biennial oscillation in the lower stratosphere can explain the circulation anomalies of the anomalously cold European winter of 1962/63 when both were in an extreme easterly phase.

1. Introduction

Variations in the tropics can affect the variability of the extratropical atmospheric circulation in many ways. The most important source of tropical influence is the El Niño–Southern Oscillation (ENSO) phenomenon. In the Pacific region, ENSO is known to strongly influence the Pacific–North American pattern [PNA; see the review by Trenberth et al. (1998)]; in particular, the Aleutian low is deepened during warm ENSO events. The tropics can also influence other circulation patterns in the extratropics, such as the southern annular mode (SAM; L'Heureux and Thompson 2006; Ding et al. 2012, 2014a,b) and the East Asian monsoon (Wang et al. 2008; Sun et al. 2010; Gollan et al. 2012). These teleconnections are sometimes seasonally varying (L'Heureux and Thompson 2006), can exhibit nonstationary behavior on decadal time scales (e.g., Greatbatch et al. 2004; Wang et al. 2008; Ding et al. 2012, 2014b,c), and sometimes involve the stratosphere in their dynamics (e.g., Ineson and Scaife 2009).

Over the Euro-Atlantic region, the dominant mode of low-frequency variability in the atmospheric circulation is the North Atlantic Oscillation [NAO; Walker and Bliss 1932; see Greatbatch (2000) and Hurrell et al. (2003) for reviews]. It has been noted that on intraseasonal time scales, the NAO interacts with the tropics via the Madden–Julian oscillation (MJO; Cassou 2008; Lin et al. 2009; Ding et al. 2010). On the other hand, Greatbatch et al. (2003, 2012a) have found that on interannual time scales the tropical influence on the NAO is, in general, rather weak and other factors may be more important such as variability internal to the extratropical atmosphere, including both the troposphere and the stratosphere, whereas on decadal time scales the tropics seem to play a more important role (Hoerling et al. 2001; Greatbatch et al. 2012a,b).

However, previous studies, using model experiments with relaxation toward reanalysis data in different regions of the atmosphere, have also shown that in certain boreal winters such as 2005/06 (Jung et al. 2010a) and

Corresponding author address: Gereon Gollan, GEOMAR Helmholtz Centre for Ocean Research Kiel, Düsternbrooker Weg 20, 24105 Kiel, Germany.
E-mail: ggollan@geomar.de

DOI: 10.1175/JCLI-D-14-00185.1

1962/63 (Greatbatch et al. 2014), the tropics can be a significant driver of the extratropical circulation in the Northern Hemisphere (NH). These authors argue that both NH winters 1962/63 and 2005/06 were likely to have been influenced by the easterly phase of the quasi-biennial oscillation (QBO). The QBO describes vertically alternating zonal wind bands in the stratosphere along the equator, propagating downward with a time scale of slightly more than two years. The QBO has a predictability of several months and its impact on the extratropical stratosphere and on the troposphere in the Euro-Atlantic region has been noted by many authors (e.g., Holton and Tan 1980; Baldwin et al. 2001; Boer and Hamilton 2008; Marshall and Scaife 2009). When the zonal winds associated with the QBO are easterly in the lower stratosphere, as during the winters 1962/63 and 2005/06, the QBO favors negative NAO regimes and cold European winters. However, this factor alone is not enough to explain the particularly extreme winter of 1962/63 (Folland et al. 2012; Greatbatch et al. 2014). Greatbatch et al. (2014) note the occurrence of anomalously strong easterly upper-tropospheric zonal-mean zonal winds along the equator during winter 1962/63 and speculate that this could, in addition to the QBO, be responsible for the strong tropical impact as seen in their relaxation experiments. We shall investigate this possibility in a more quantitative way in this study.

Following Nigam (1990), tropospheric zonal-mean zonal wind $[U]$ (where U is the zonal wind and the square brackets denote the zonal average) will first be examined in detail in the present paper by using a rotated empirical orthogonal function analysis applied to $[U]$ at all latitudes. We find a mode of $[U]$ variability centered over the equator in the upper troposphere, linearly independent of ENSO and the QBO, but related to the MJO, consistent with previous studies (Slingo et al. 1996; Hoskins et al. 1999; Kraucunas and Hartmann 2005). The corresponding time series is found to be highly correlated with $[U]$ at 150 hPa averaged between 5°N and 5°S (hereafter denoted $[\mathrm{U150}]_E$, where the E subscript indicates "equatorial"). Then, regression analysis using $[\mathrm{U150}]_E$ reveals significant influence on middle tropospheric circulation anomalies on monthly to interannual time scales in the extratropical NH in boreal winter. The results are confirmed using a model experiment in which the tropical atmosphere, and therefore also $[\mathrm{U150}]_E$, is relaxed toward the 40-yr European Centre for Medium-Range Weather Forecasts (ECMWF) Re-Analysis (ERA-40; Uppala et al. 2005) data, as in Greatbatch et al. (2012a) and Greatbatch et al. (2014). A parallel comparing analysis of the extratropical influence of the QBO, and of the linearly combined influences of the QBO and $[\mathrm{U150}]_E$ is also carried out.

The structure of the present paper is as follows. In section 2 we describe the datasets and the model experiment we use. We show the results from the RPC analysis in section 3, together with some tests on their robustness and an assessment regarding the forcing of $[\mathrm{U150}]_E$. In section 4, we present a regression analysis, using $[\mathrm{U150}]_E$, on 500-hPa geopotential height to study the impact of this mode on the extratropical circulation and discuss possible mechanisms for this influence by investigating changes in the subtropical waveguides and Rossby wave sources associated with $[\mathrm{U150}]_E$. An application of the results to the winter of 1962/63 is then presented in section 5. We finish with a summary and discussion in section 6.

2. Data and model

To ensure the robustness of our results, three different reanalysis datasets are used here:

- the National Centers for Environmental Prediction–National Center for Atmospheric Research (NCEP–NCAR) reanalysis starts in January 1948 and is continuously updated (Kalnay et al. 1996),
- the ERA-40 reanalysis is a complete dataset that extends from September 1957 to August 2002 (Uppala et al. 2005), and
- the ECMWF Interim Re-Analysis (ERA-Interim) starts with the beginning of the satellite era in 1979 and is also continuously updated (Dee et al. 2011).

We make use of U at all standard pressure levels between 1000 and 100 hPa, geopotential height at the 500-hPa level (Z500), and total outgoing longwave radiation (OLR), as well as the divergence D and relative vorticity ξ at 200 hPa. The National Oceanic and Atmospheric Administration (NOAA) Extended Reconstructed Sea Surface Temperature (ERSST) data, version 3b (V3b), are used to compute the Niño-3.4 index following the recipe described at http://www.cgd.ucar.edu/cas/catalog/climind/TNI_N34/index.html. The monthly-mean climatology is removed before all analyses, if not stated otherwise, and is computed separately for each dataset.

Results from model simulations carried out with the ECMWF model are also discussed (see Jung et al. 2010b). These simulations use a relaxation technique, in which the dynamical variables (U, V, T, and p_s)[1] are relaxed toward the ERA-40 reanalysis within the tropical atmosphere at all vertical levels (see Greatbatch et al. 2012a). In this way, the zonal winds in the upper

[1] Zonal velocity is U, meridional velocity is V, air temperature is T, and surface pressure is p_s.

tropical troposphere, but also all other variability in the tropical atmosphere including the QBO, are effectively prescribed by the relaxation, and the extratropical response in the model can be compared with results obtained from the ERA-40 reanalysis. The relaxation in our experiment is confined laterally from 20°S to 20°N, including a smooth transition zone between relaxed and unrelaxed parts of the model domain (see Greatbatch et al. 2012a). Climatological SST and sea ice, computed for the period 1979–2002, are prescribed at the lower boundary and radiative forcing does not change interannually. This is the experiment CLIM-TROPICS in Greatbatch et al. (2012a) and we continue to use this label here. The simulations cover each boreal winter from 1960/61 to 2001/02 and have all been initialized on or around 1 November and then run until the end of February. Twelve realizations are integrated for each winter, each using different initial conditions from around November 1st. Having 12 realizations of the experiment for each winter, it is possible to extract the forced signal from the noise by averaging over the whole ensemble. Model anomalies refer to deviations from the model climatology to reflect anomalous circulation states rather than the difference between the model climate and the reanalysis climate.

3. Analysis of the zonal-mean zonal wind

a. *Results of the rotated empirical orthogonal functions analysis*

Nigam (1990, hereafter N90) has analyzed tropospheric $[U]$ at all latitudes ϕ during a 9-yr period (1980–88) using a rotated empirical orthogonal function (REOF) analysis [as described, e.g., by von Storch and Zwiers (2001)]. N90 used the varimax rotation method, which makes the structure of the resulting patterns more regionally confined and at the same time more physically meaningful. Doing a classic empirical orthogonal function (EOF) analysis on $[U]$ reveals unrealistic and patchy patterns with signatures in both hemispheres, without the simple physical interpretation we are able to give the REOFs below. N90 found four dominant modes of variability, but also made the remark that the data record was too short to make any definite conclusions from findings regarding the third and fourth modes. The first two modes in N90 represent fluctuations of the midlatitude jets in the northern and southern extratropics respectively, while he associated the third and fourth modes with variations of deep convection in the tropics. We update his REOF analysis with nearly the same methods, but using the longer reanalysis datasets for the December, January, and February monthly-mean anomalies of $[U]$ on standard pressure levels from 1000 to 100 hPa (see section 2). The $[U]$ anomalies have been weighted before the REOF analysis, according to area $[\sqrt{\cos(\phi)}]$ and mass, depending on the pressure interval represented by the data. Our only addition to the methods of N90 (at least this detail was not noted in N90) is that we remove the linear trend from $[U]$ before the analysis. Furthermore, as the signs of EOFs on which the REOF analysis is based are arbitrary, we invert the sign of a given mode pattern (referred to as REOF hereafter) and the corresponding principal component time series (referred to as RPC hereafter) if the mode pattern only contains a monopole with a negative amplitude. In such a way the interpretation is more intuitive, as a positive index then refers to westerly wind anomalies. The order of the modes is defined by the percentage of variance they explain in the global $[U]$ that the analysis is based on, while it should be noted that the explained variances of the rotated modes are not additive, in contrast to those of the original EOFs. Also, the RPC time series are not completely uncorrelated by definition, again in contrast to the principal components of a classic EOF analysis.

Our Fig. 1 shows the first four modes (REOF1–REOF4 hereafter) of our analysis for NCEP–NCAR December–February (DJF) monthly-mean data from December 1949 to February 2013 (climatological monthly means removed). Also plotted in light contours is the climatological zonal-mean zonal wind, mainly showing the midlatitude westerly jets. Not visible because of the large contour interval for the climatology are the negative $[U]$ values corresponding to the easterly trade winds in the lower troposphere on both sides of the equator. At the equator, the climatological mean upper-tropospheric $[U]$ is near zero.

Table 1 shows the correlations between the monthly-mean principal component time series (Fig. 1, right) and some prominent large-scale circulation indices. As in N90, the two leading modes represent meridional fluctuations of the extratropical jets with a quasi-barotropic structure. The first mode is related to the northern annular mode (NAM) and explains about 17% of the global variance in $[U]$; its RPC time series is strongly positively correlated with the NAM index defined by Thompson and Wallace (2000) (see Table 1). Similarly for the Southern Hemisphere extratropics, the second REOF mode represents 14% of the global variance in $[U]$ and is strongly negatively correlated with the SAM index (Thompson and Wallace 2000).

Modes 3 and 4 have a much more distinct structure compared to those presented in N90. While N90's modes 3 and 4 have signatures in both the tropics and in the extratropics, we find two exclusively tropical modes. It has to be noted that our modes 3 and 4 represent nearly the same amount of variance in $[U]$, indicating that they

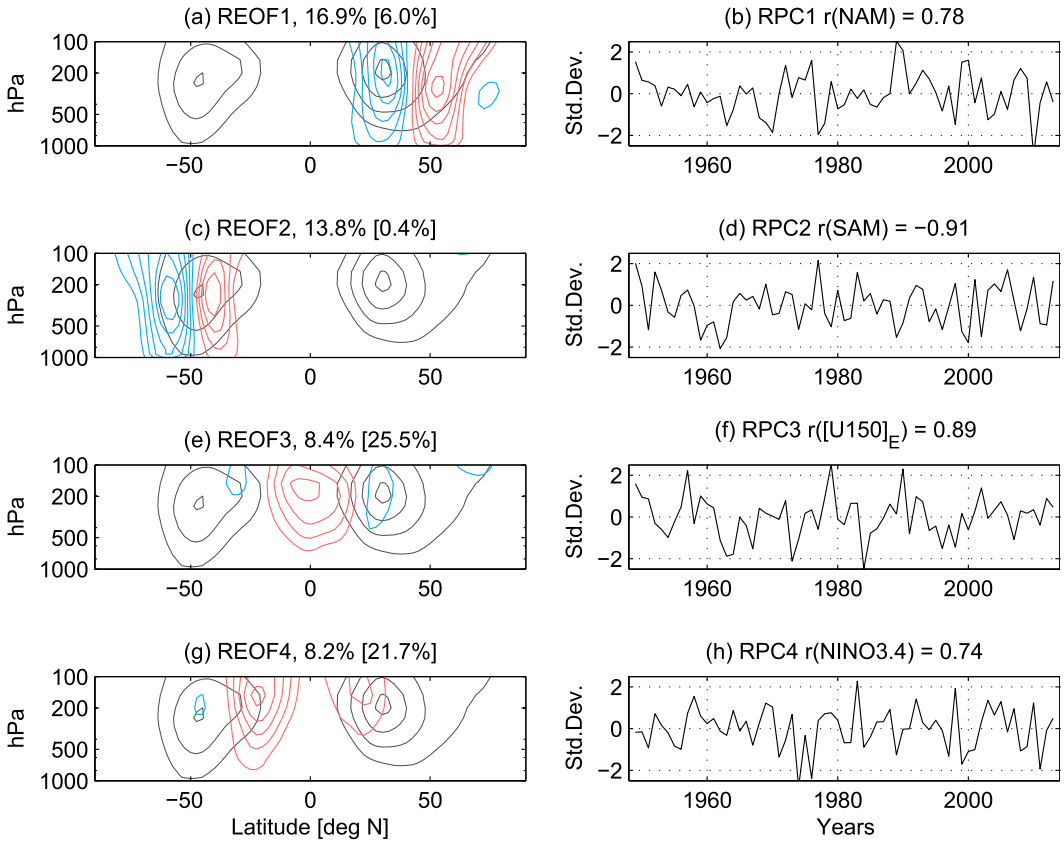

FIG. 1. (left) The first four modes from an REOF analysis using DJF monthly-mean $[U]$ anomalies from NCEP–NCAR. Red and blue contours show the loading patterns corresponding to plus one standard deviation of the RPC time series in descending order of explained variance in the original data. The contour interval is 0.5 m s^{-1} and red (blue) contours refer to positive (negative) values, while the zero contour is omitted. Additionally, the climatological $[U]$ for DJF is shown in gray contours with a contour interval of 10 m s^{-1}, again without zero contour. The explained variance is given in percent in the header of each panel in (left), and the explained variance of the mode within the tropics (25°N/S) is given in brackets. (right) The RPC time series in units of standard deviation and, instead of the monthly means used for the analysis, the DJF means are plotted; years are labeled according to the January dates. Also given in the header of each panel are the highest correlations between the monthly-mean time series and the climate indices listed in Table 1.

are of roughly equal importance. However, as we show below, both modes have a physically distinct interpretation and hence, we believe, are not artifacts of the REOF analysis.

The third mode (REOF3) has a quasi-monopole pattern centered in the upper troposphere (between 150 and 200 hPa) over the equator and explains about 8% of the variance of $[U]$ globally. Within the tropics between 25°N and 25°S it explains about 25% of the variance of $[U]$ (shown in brackets in the title of Fig. 1e) and is the leading mode there (discussed below). Its structure is baroclinic with no amplitude at the surface and its time series (RPC3) is not correlated with any of the NAM, SAM, Niño-3.4, or QBO indices (see Table 1). This mode describes changes between easterlies and westerlies in a region where the climatology of $[U]$ in DJF is near zero. As already stated in the introduction, the time series RPC3 is highly correlated with $[\mathrm{U150}]_E$, to be discussed in more detail later.

RPC4, on the other hand, is highly correlated with the Niño-3.4 index ($r = 0.74$) and REOF4 has a signature in $[U]$ in the regions of the subtropical jets on both sides of the equator. Warm ENSO events (positive Niño-3.4 index) cause more upper-tropospheric divergence in the equatorial region and upper-tropospheric poleward flow, transporting angular momentum poleward in both hemispheres and therefore accelerating the subtropical jets (e.g., Held and Hou 1980; Oort and Yienger 1996; Seager et al. 2003). Furthermore, the structure of REOF4 is consistent with the response to a zonally symmetric deep equatorial heating in a model with a climatological zonal-mean basic flow (Hoskins et al. 1999).

TABLE 1. Correlations r between the monthly DJF time series of the REOF analysis and selected climate indices: Niño-3.4 was computed using the recipe described at http://www.cgd.ucar.edu/cas/catalog/climind/TNI_N34/index.html and NOAA ERSST V3b data. The QBO indices are zonal-mean zonal wind anomalies averaged between 10°S and 10°N at 30 hPa (QBO30) and at 50 hPa (QBO50), respectively, both normalized by their standard deviation. The NAM index has been calculated using geopotential height at 850 hPa following Thompson and Wallace (2000) (SAM index analog for the Southern Hemisphere). All data are from NCEP–NCAR reanalysis for winters 1949–2013. All indices have been detrended in advance. The highest correlations for each mode are highlighted in boldface, which are all significantly different from zero at the 95% level.

	Niño-3.4	QBO30	QBO50	NAM	SAM	$[U150]_E$
RPC1	−0.33	0.12	0.01	**0.80**	0.05	0.16
RPC2	0.32	−0.12	−0.10	−0.01	**−0.91**	−0.05
RPC3	−0.07	−0.07	−0.11	−0.01	0.05	**0.89**
RPC4	**0.74**	−0.03	0.09	−0.20	−0.19	0.15
$[U150]_E$	−0.11	−0.10	−0.10	−0.06	0.03	1

Dommenget and Latif (2002) note that the results of EOF analyses, including rotated EOF analyses, have to be interpreted with caution as they need not be physically meaningful, because of the requirements of the methods, such as the orthogonality of EOF patterns (also the case for the varimax method used here). Since REOF1, REOF2, and REOF4 all represent known phenomena with a physical interpretation, we compare REOF3 to the simple index $[U150]_E$ in Fig. 2. In this case, the REOF analysis was applied to detrended monthly-mean data over the full year and gives a similar REOF3 pattern as in Fig. 1. It can also be deduced from Table 2 that the RPC3 time series based on the REOF analysis applied to the whole year is very similar in DJF to the RPC3 time series obtained from the REOF analysis applied to DJF monthly-mean data. Figure 2 shows both the time series of $[U150]_E$, normalized by its standard deviation, and its regression onto the global $[U]$ in comparison with the REOF3 pattern. For both indices in Fig. 2, detrended monthly-mean anomalies of $[U]$ over the full year were used from NCEP–NCAR data between 1949 and 2012. The regression pattern associated with $[U150]_E$ has a very similar shape, with slightly enhanced amplitude compared to the REOF3 pattern. Furthermore, the correlation between the two time series is very high ($r = 0.91$) and also the characteristics of the autocorrelation functions (Fig. 2c) of $[U150]_E$ and RPC3 are very similar. Using the e-folding time scale of the autocorrelation function, we get a decorrelation time of about two months for both the RPC3 and the $[U150]_E$ indices, implying at least some potential for medium-range

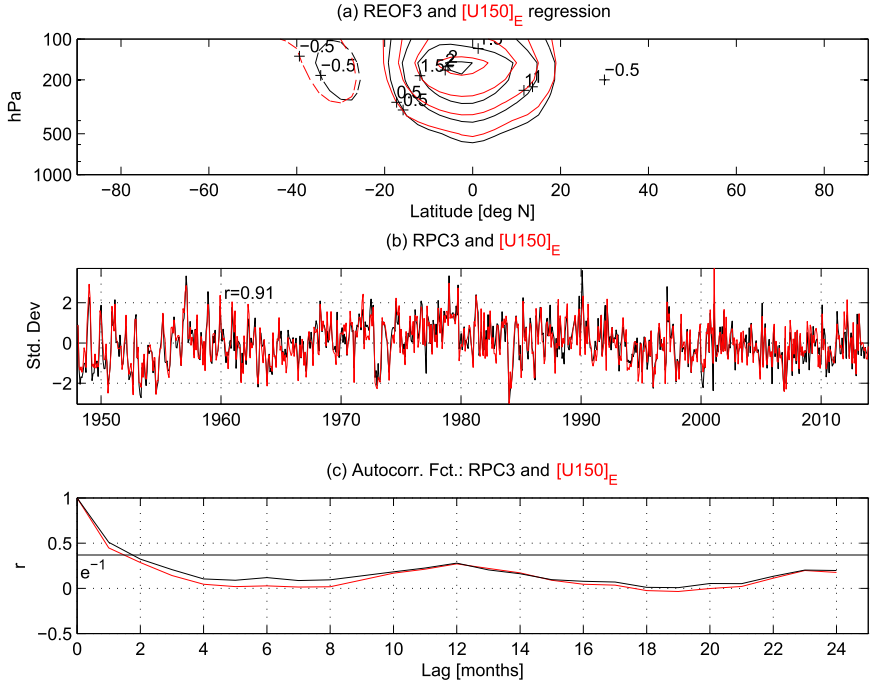

FIG. 2. (a) The REOF3 loading pattern as in Fig. 1, but computed using monthly-mean anomalies from the whole year (black) and the regression of $[U]$ from NCEP–NCAR onto the monthly-mean $[U150]_E$ index (red). The contour interval is 0.5 m s^{-1}. (b) The corresponding monthly time series of RPC3 ($[U150]_E$) in black (red) normalized to one standard deviation. (c) The autocorrelation functions for the two time series. The e-folding time scales are reached when the autocorrelation functions cut the horizontal black line.

TABLE 2. REOF modes that are highly correlated to $[U150]_E$, based on REOF analysis using the datasets ERA-40, ERA-Interim, and NCEP–NCAR with different time periods: monthly anomalies, seasonal anomalies, and an REOF analysis carried out on monthly anomalies over the whole year (i.e., full year). For each combination the rank of the mode is given (first column), as well as the explained variance (second column) and the correlation r between the corresponding RPC time series and $[U150]_E$ from ERA-40 (third column) during the overlapping period. Shown in brackets are the respective numbers for the same REOF analysis restricted to tropical latitudes $\phi \leq 25°$N/S). For each dataset, the correlation between $[U150]_E$ from ERA-40 and $[U150]_E$ from each dataset is also given, referring to the full year monthly time series during each overlapping period. REOF3 from Fig. 1 is highlighted in boldface.

	Rank	Explained variance (%)	$r([U150]_{E,\mathrm{ERA-40}})$
ERA-40			
DJF monthly	3rd [1st]	13.4 [25.3]	0.84 [0.85]
Full year	2nd [1st]	12.2 [21.9]	0.86 [0.87]
DJF seasonal	3rd [2nd]	13.9 [23.8]	0.78 [0.82]
$[U150]_{E,\mathrm{ERA-40}}$	—	—	1
ERA-Interim			
DJF monthly	5th [2nd]	8.6 [22.9]	0.78 [0.79]
Full year	5th [1st]	7.3 [21.4]	0.83 [0.84]
DJF seasonal	5th [3rd]	7.5 [18.2]	0.52 [0.67]
$[U150]_{E,\mathrm{ERA-Interim}}$	—	—	0.94
NCEP–NCAR			
DJF monthly	**3rd [1st]**	**8.4** [24.6]	**0.74** [0.72]
Full year	3rd [1st]	8.5 [22.3]	0.74 [0.79]
DJF seasonal	5th [2nd]	7.7 [21.5]	0.76 [0.74]
$[U150]_{E,\mathrm{NCEP-NCAR}}$	—	—	0.79

predictability. There is also a hint of an annual memory/periodicity in the autocorrelation function, but possible reasons for this are not discussed in the present paper. Given the similarity between $[U150]_E$ and RPC3 and the simple definition of $[U150]_E$ compared to that of RPC3, the former is used for the analysis in the rest of the paper.

Figure 3 shows a comparison between the $[U150]_E$ indices from NCEP–NCAR, ERA-40, and ERA-Interim data showing winter (DJF) seasonal mean anomalies for convenience. QBO indices (computed at 30 hPa) are also shown, since these will be referred to later in this study. As noted in Table 1, $[U150]_E$ is weakly anticorrelated with the Niño-3.4 index in the NCEP–NCAR reanalysis, which is also true for the ECMWF reanalyses. To remove any unwanted effect of ENSO in our following composite and regression analyses, we remove variations from the $[U150]_E$ index that are linearly dependent of ENSO, as measured by the Niño-3.4 index. All time series are normalized to have unit standard deviation σ—note that $\sigma([U150]_E)$ is about 1.7 m s^{-1} and σ(QBO30) is about 10 m s^{-1}. The normalized time series with ENSO effects removed is hereafter denoted as $\widehat{[U150]}_E$. In the overlapping period (December 1957–February 2002) the monthly $[U150]_E$ indices from NCEP–NCAR and ERA-40 data are correlated highly at almost $r = 0.8$ (see also Table 2). However, it can be seen from the different $\widehat{[U150]}_E$ time series that the wind data at the upper troposphere over the equator are sometimes uncertain, as the amplitude can differ between the reanalyses, especially in winters during the presatellite era, and even the sign is uncertain in winters like 1959/60, 1980/81, and 1998/99. The standard "reference index" for analysis in this paper will be the monthly-mean DJF $[U150]_E$ (and also $\widehat{[U150]}_E$ as noted in the text) from ERA-40 (climatological monthly means removed). This is because we want to ensure comparability with the model results, which use ERA-40 for the relaxation within the tropics.

We further analyze the robustness of our REOF analysis with respect to the different reanalysis datasets and to slightly different methods or time periods used

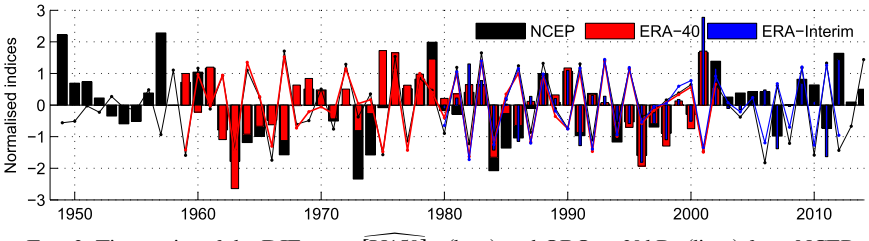

FIG. 3. Time series of the DJF mean $\widehat{[U150]}_E$ (bars) and QBO at 30 hPa (lines) from NCEP–NCAR (black), ERA-40 (red), and ERA-Interim (blue) datasets. Years are labeled according to January dates and all time series are detrended and normalized to have a standard deviation of one.

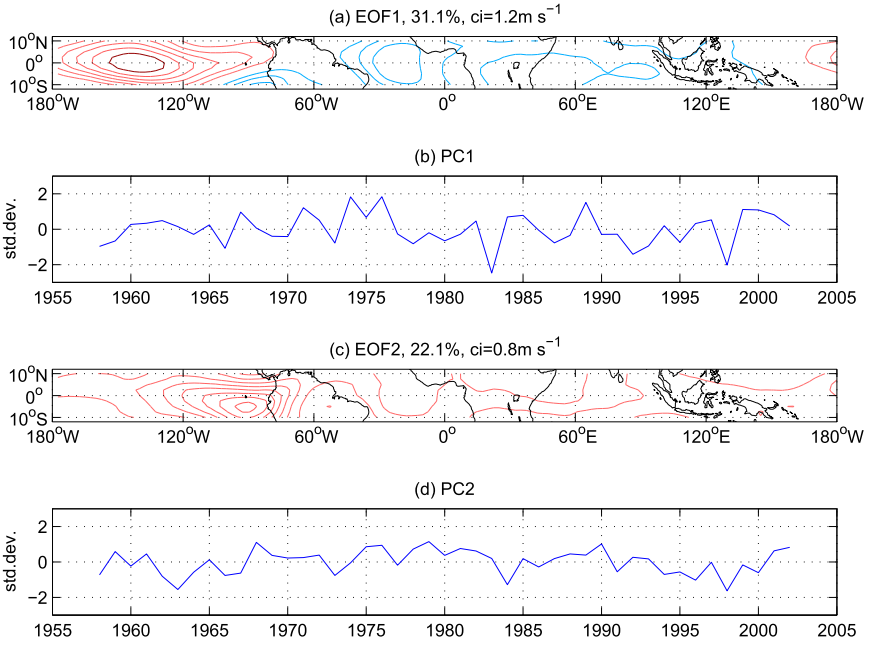

FIG. 4. The first two EOF modes using DJF monthly anomalies of U200 from ERA-40 at all longitudes between 10°N and 10°S. (a),(c) The first and second loading patterns with red (blue) contours indicating positive (negative) anomalies. The contour intervals (ci) are different for the two loading patterns and are indicated in the title of the panel, while the zero contour is always omitted; the explained variances in percent are also given in the titles. (b),(d) The corresponding time series in units of standard deviations. The correlations between U200-PC1 and Niño-3.4 and between U200-PC2 and $[U150]_E$ are −0.81 and 0.92, respectively (see Table 3).

for the analysis. Data from ERA-40, ERA-Interim, and NCEP–NCAR are tested, as well as using DJF mean anomalies or monthly-mean anomalies of $[U]$ over the full year for the REOF analysis. Furthermore, we have performed the same set of REOF analyses, but restricted to tropical latitudes ($\phi \leq 25$°N/S). For each case, the correlation between the RPC time series and the reference index $[U150]_E$ from ERA-40 during the overlapping period is also computed. The results are noted in Table 2 for the REOF mode whose RPC time series has the highest correlation with the $[U150]_E$ index from ERA-40. These correlations are generally very high (note the variable overlap; i.e., 23 yr for ERA-Interim and 45 yr for NCEP–NCAR reanalysis). The results of Table 2 can be summarized by saying that the mode related to $[U150]_E$ always occurs as one of the second to fifth REOF modes and that the explained variance of this mode is always between 8% and 13%. When restricting the REOF analysis to the tropics, this mode occurs as the first or second mode and explains about 20%–25% of the variance there. Additionally the correlations between the reference index and $[U150]_E$ from ERA-Interim and NCEP–NCAR reanalysis are also given in Table 2.

The first two modes from an EOF analysis applied to monthly-mean data for DJF of U at 200 hPa (U200) between 10°N and 10°S (hereafter U200-EOF1 and U200-EOF2), using ERA-40 data, are shown in Fig. 4 together with the corresponding time series U200-PC1 and U200-PC2. Notably, the first mode represents the modulation of the Walker circulation due to ENSO variability, explaining about 30% of the total variance of U200 between 10°N and 10°S. The correlation between U200-PC1 and the Niño-3.4 index is −0.81 (see Table 3). On the other hand, U200-EOF2 represents variations of U200 (about 20% of the total variance) with the same sign over the whole domain and with strongest variations over the eastern tropical Pacific. The time series U200-PC2 is highly correlated ($r = 0.92$) with $[U150]_E$, which in turn indicates that significant zonal variation is related to variability of the $[U150]_E$ index and in particular that the wind anomalies associated with $[U150]_E$ are largest over the eastern tropical Pacific. In section 4b we will further discuss the importance of wind anomalies in the eastern tropical Pacific for the extratropical influence of $[U150]_E$.

b. *Mechanisms for upper-tropospheric anomalies of $[U]$ at the equator*

As shown by previous studies (e.g., Hoskins et al. 1999; Lee 1999; Kraucunas and Hartmann 2005), zonally asymmetric tropical diabatic heating can lead to westerly

TABLE 3. Correlations r between the PC time series for an EOF analysis applied to ERA-40 U200 between 10°N and 10°S (shown in Fig. 4) and the Niño-3.4 and $[U150]_E$ indices. The highest correlation for each mode is highlighted in boldface, which is also significantly different from zero at the 95% level.

	Niño-3.4	$[U150]_E$
U200-PC1	**−0.81**	0.05
U200-PC2	−0.16	**0.92**

acceleration of $[U]$ in the upper equatorial troposphere if the heating is located so that there is an associated eddy flux of westerly momentum toward the equator. The westerly acceleration is balanced by downward fluxes of momentum and by the zonal-mean meridional overturning circulation, both removing westerly momentum from the equatorial upper troposphere (Kraucunas and Hartmann 2005). A localized heating is provided, on intraseasonal time scales, by the heating centers of the MJO, which can both accelerate and decelerate upper equatorial $[U]$, depending on the phase of the MJO, resulting from the interaction of the circulation generated by the heating anomaly and the climatological stationary waves (Hoskins et al. 1999).

A simple analysis is shown in Fig. 5, using the daily real-time multivariate MJO (RMM) indices by Wheeler and Hendon (2004) (indices are taken from http://cawcr.gov.au/staff/mwheeler/maproom/RMM/RMM1RMM2.74toRealtime.txt), where RMM1 and RMM2 are the time series of the first two multivariate EOFs (using normalized tropical OLR, zonal wind at 850 hPa, and U200) and $|\text{MJO}| = \sqrt{\text{RMM1}^2 + \text{RMM2}^2}$ is the MJO amplitude. The MJO is evaluated against the monthly $\widehat{[U150]}_E$ index from ERA-Interim, both datasets covering the time period DJF 1979–2012.

First in Fig. 5a, the activity of the MJO is evaluated against the phase of $\widehat{[U150]}_E$. More days of active MJO occur during months with westerly $\widehat{[U150]}_E$, whereas there are clearly more days of inactive MJO during months of easterly $\widehat{[U150]}_E$. Additionally, the evaluation of the different MJO phases shows quite clearly that westerly $\widehat{[U150]}_E$ is preferred when the MJO is in late phases (phase 7) and easterly $\widehat{[U150]}_E$ is preferred when the MJO is in early phases (phases 3 and 4). However, on most days of months with easterly $\widehat{[U150]}_E$, the MJO is inactive as shown by Fig. 5a. Put together, these results are another observational confirmation of conclusions from previous authors regarding the MJO forcing of equatorial upper-tropospheric $[U]$ (e.g., Hoskins et al. 1999; Lee 1999; Kraucunas and Hartmann 2005).

Furthermore, hemispherically asymmetric tropical heating leads to an easterly acceleration of $[U]$ over the

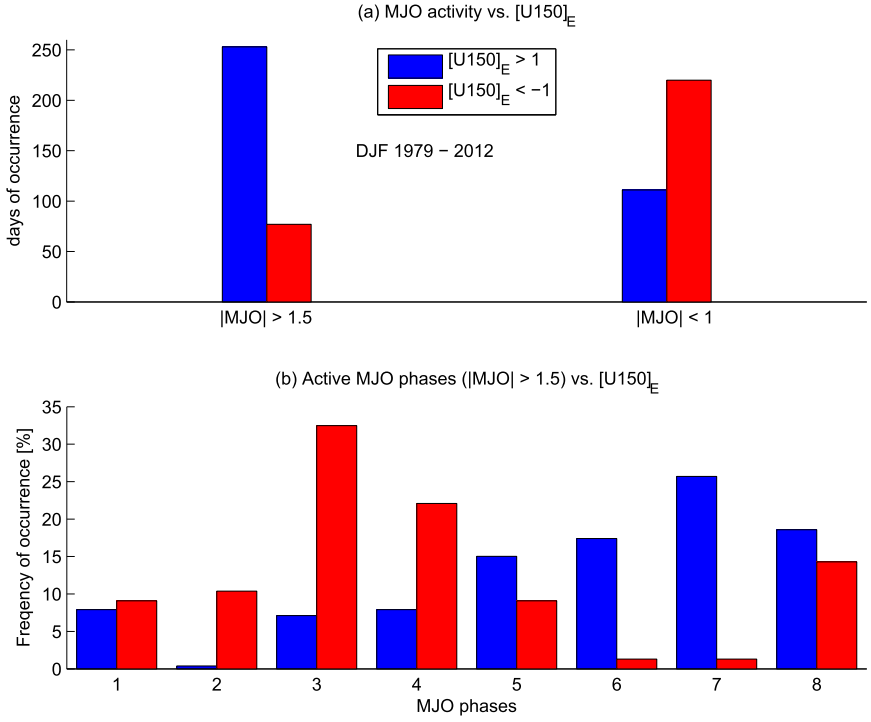

FIG. 5. Evaluation of monthly $\widehat{[U150]}_E$ from ERA-Interim against daily MJO ($|\text{MJO}| = \sqrt{\text{RMM1}^2 + \text{RMM2}^2}$, see text for data source), both over the period DJF 1979–2012. (a) Days of active ($|\text{MJO}| > 1.5$) and inactive ($|\text{MJO}| < 1$) MJO during months of $\widehat{[U150]}_E > 1$ (blue) and $\widehat{[U150]}_E < -1$ (red). (b) Frequency of occurrence of active MJO phases during months of $\widehat{[U150]}_E > 1$ (blue) and $\widehat{[U150]}_E < -1$ (red).

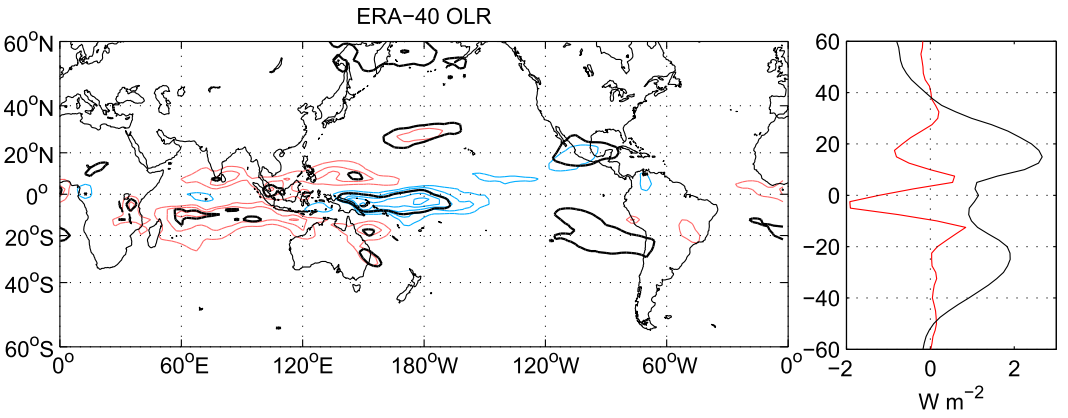

FIG. 6. (left) Regressions onto the $\widehat{[U150]}_E$ index using monthly-mean ERA-40 OLR anomalies for DJF, where red (blue) contours refer to positive (negative) OLR anomalies with a contour interval of 2 W m^{-2}. The zero contour is omitted and black contours encircle areas where the correlation is significantly different from zero at the 95% level. (right) The zonal mean of the regression map (red), together with the zonal-mean OLR climatology from ERA-40 (black). The global mean (227.9 W m^{-2}) is subtracted from the climatology and the result is scaled by 20^{-1}.

equator due to the advection of easterly angular momentum by the associated cross-equatorial flow (e.g., Lee 1999). This is evident during boreal summer, when the tropical heating zone is displaced into the Northern Hemisphere and climatological $[U]$ is strongly easterly in the upper troposphere over the equator, whereas during boreal winter, when the heating zone is only slightly south of the equator, climatological $[U]$ is near zero there. Figure 6 shows the regression map of monthly-mean OLR anomalies from ERA-40 for DJF onto the reference $\widehat{[U150]}_E$ index together with the zonal mean of this map. The equatorial minimum in the zonal-mean OLR climatology (black) shows the maximum in cloud cover (or, equivalently, diabatic heating) of the intertropical convergence zone. In turn, the zonal-mean regression (red) indicates that easterly $\widehat{[U150]}_E$ anomalies are associated with tropical heating anomalies that strengthen the slight climatological asymmetry in the zonal-mean tropical heating. Additionally, the OLR regression map associated with westerly $\widehat{[U150]}_E$ shows a similar structure as the patterns associated with late MJO phases, consistent with Fig. 5.

4. Circulation anomalies associated with $[U150]_E$

a. *Regression analysis for ERA-40 data and model output*

As seen from its autocorrelation function, $[U150]_E$ may be predictable to some extent, or at least persists on longer time scales than synoptic variability in the extratropics. In this section we discuss a possible impact on the extratropical circulation with potential implications for medium-range to seasonal forecasting. Previous studies showed that the stratospheric equatorial zonal wind (i.e., the QBO) has good predictability because of its periodicity and also has an impact on the extratropics (e.g., Holton and Tan 1980; Marshall and Scaife 2009). Indeed, the QBO has been shown to be valuable for medium-range to seasonal predictions of the extratropical circulation (e.g., Boer and Hamilton 2008; Folland et al. 2012). Here we want to compare the influence of the QBO and variability associated with $[U150]_E$ by means of a regression analysis while noting that the QBO and $[U150]_E$ indices are uncorrelated with each other (see Table 1). Since $[U150]_E$ is weakly (not significantly) anticorrelated with the Niño-3.4 index and is therefore not completely independent, we use the index $\widehat{[U150]}_E$ with ENSO influences linearly removed.

The linear regression of ERA-40 DJF monthly-mean anomalies of Z500 onto the reference $\widehat{[U150]}_E$ index is shown in Fig. 7a. The same is shown in Fig. 7c for the QBO index at 30 hPa (QBO30; see also Fig. 3). Additionally, we compare the regression patterns with the corresponding results using data from the relaxation experiment CLIM-TROPICS in Figs. 7b and 7d. The results of the regressions are similar when using NCEP–NCAR data, but we continue with ERA-40 data here. Also, similar results are obtained by calculating composites (averaging over months with the $\widehat{[U150]}_E$ index being larger than 1 and those smaller than −1) instead of regressions.

In the ERA-40 regression, associated with the westerly phase of $\widehat{[U150]}_E$, there is a band of positive Z500 anomalies from central Asia to the eastern Pacific at low to middle latitudes and negative Z500 anomalies north of this band over the western North Pacific. Therefore, the trough associated with the Aleutian low is shifted to the north during the westerly phase of $\widehat{[U150]}_E$,

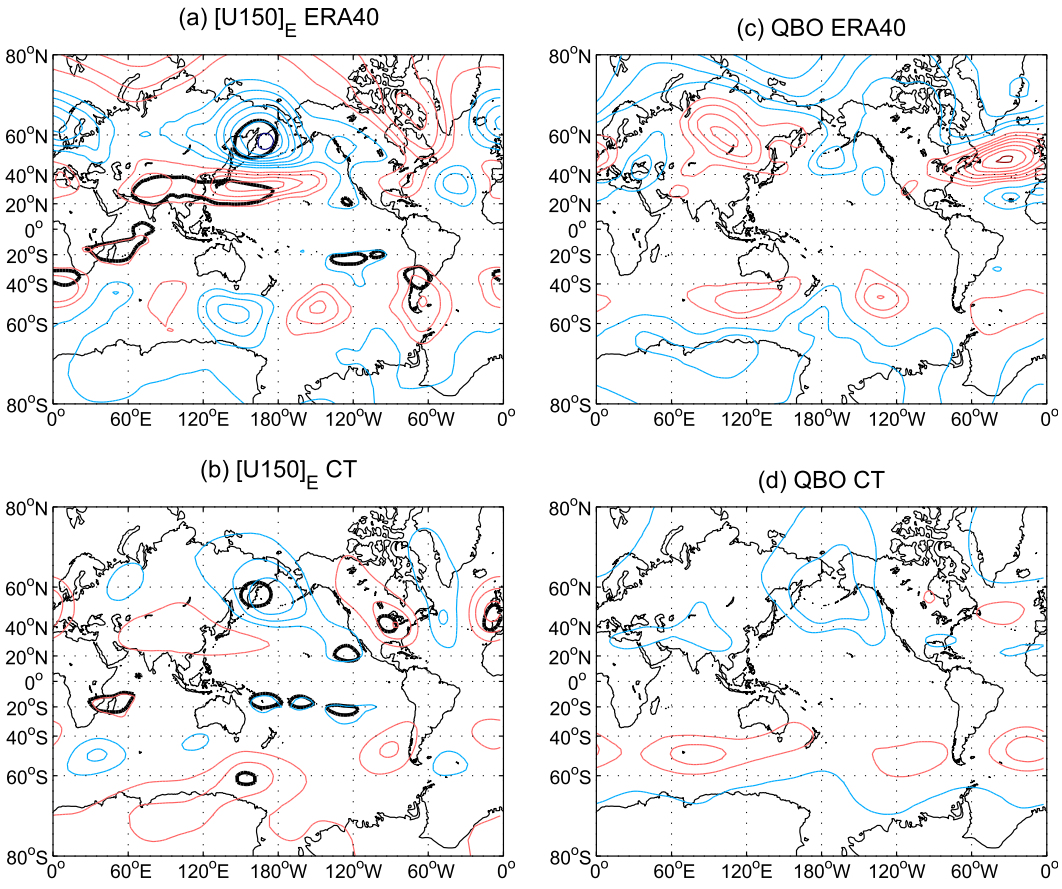

FIG. 7. (a) Regression of the DJF monthly-mean anomalies of Z500 onto the monthly $\widehat{[U150]}_E$ time series, both from ERA-40. (b) As in (a), but for Z500 anomalies from the ensemble mean of the relaxation experiment CLIM-TROPICS (CT). (c),(d) The corresponding regressions for the QBO index computed at 30 hPa. The contour interval in each panel is 3 m with red (blue) contours indicating positive (negative) anomalies, while the zero contour has been omitted and black contours encircle areas where the correlation is significantly different from zero at the 95% level.

causing a slightly weakened East Asian jet stream. In the Southern Hemisphere there is a similar, but less continuous, band of positive Z500 anomalies at subtropical latitudes and negative Z500 anomalies poleward of this band. However, the regressions are not significant in most regions in the Southern Hemisphere and the anomalies do not agree when comparing the ERA-40 and the CLIM-TROPICS regression. Over the Atlantic and the polar regions (the latter not shown here) a patchy structure can be found with a positive anomaly over the east of North America toward the North Pole and negative anomalies over the subtropical North Atlantic and over northern Europe. The regression of Z500 is significant at the 95% level over the western North Pacific and East Asia, whereas over the Atlantic/European region it is not. The results for the Euro-Atlantic sector and the Southern Hemisphere are consistent with the lack of correlation between the $[U150]_E$ index and the NAM and the SAM time series noted earlier (see Table 1).

To get more insight into the tropically forced extratropical circulation associated with $\widehat{[U150]}_E$, we now use the ensemble mean of the relaxation experiment CLIM-TROPICS for the regressions of Z500. As the tropically forced extratropical signal is filtered from the extratropical noise (as represented by the internal variability associated with the individual ensemble members) by taking the ensemble mean, the regression patterns are cleaner and of smaller amplitude than for the ERA-40 data (Figs. 7b,d). In the model, the signal associated with $\widehat{[U150]}_E$ (Fig. 7b) over the North Pacific and East Asia is weaker than in the reanalysis and is no longer significant over subtropical East Asia, but retains its spatial structure. In the Southern Hemisphere, we do not find consistent patterns when comparing the regressions of CLIM-TROPICS and ERA-40. Interestingly, the anomaly centers over the North Atlantic are statistically significant using the model data and now reveal a wave train from the eastern Pacific across the North Atlantic toward

Europe. The wave train can also be seen in the regression pattern from ERA-40, slightly farther south than in the model and with some distortion. Furthermore, the wave train in the model results projects onto the east Atlantic pattern (e.g., Barnston and Livezey 1987; Moore and Renfrew 2012). Possible reasons for this wave train feature will be discussed in section 4b.

We also note here that in the lower stratosphere (e.g., represented by 50-hPa geopotential height; not shown), there is the suggestion of a slight shift of the polar vortex in the NH toward the Eastern Hemisphere associated with the positive $\widehat{[\mathrm{U150}]}_E$ index and in the model a hint of the wave train identified in Fig. 7b. Overall, $[U]$ in the upper equatorial troposphere seems to be an important factor for the extratropical tropospheric circulation over both the western North Pacific and the North Atlantic and western European regions. We shall investigate possible mechanisms for the extratropical influence in section 4b.

Now we turn to the extratropical influence of the QBO for comparison. The canonical influence of the QBO on the extratropical troposphere in boreal winter favors a positive (negative) NAO pattern during the westerly (easterly) phase of the QBO. The mechanism for this effect is thought to be as follows [e.g., as described by Holton and Tan (1980)]. During the westerly phase, the zero wind line of $[U]$ in the stratosphere is shifted to the south, causing fewer stationary waves to be reflected toward the pole, leading to a cooler and stronger polar vortex in the stratosphere (Holton and Tan 1980; Baldwin et al. 2001). A stronger polar stratospheric vortex in turn favors a positive NAM/NAO regime in the troposphere (e.g., Baldwin and Dunkerton 2001). This is confirmed by our Fig. 7c, where the regression of ERA-40 Z500 onto the ERA-40 QBO30 index shows, corresponding to the westerly phase of QBO30, a pattern of deepened geopotential over the North Pole extending from Greenland to the Aleutians and enhanced geopotential over the North Atlantic where it projects onto the positive NAO pattern, even though the regression is not significantly different from zero at the 90% level. Reasons for the lack of significance could be that the downward control of the polar vortex only works efficiently in winters with stratospheric warming events. There is also large interannual variability in the winter tropospheric circulation and decadal variations in the link between QBO and the stratospheric polar vortex (see Lu et al. 2014), which can weaken the link between the QBO and the NAO. For the ensemble mean of the experiment CLIM-TROPICS (Fig. 7d), the regression has a similar pattern as for the reanalysis, but with a strongly reduced amplitude compared to the reanalysis case. Overall, the canonical extratropical influence of the QBO is confirmed by our linear regression analysis.

b. *Mechanisms for the influence of* $[\mathrm{U150}]_E$ *on the extratropical circulation*

In this section we want to discuss possible mechanisms for the extratropical influence of $[\mathrm{U150}]_E$ and, in particular, for the wave train identified over the North Atlantic. In a theoretical barotropic case, representative of the upper troposphere, the propagation of Rossby waves is controlled by so-called waveguides, which are determined by the background zonal flow (Hoskins and Ambrizzi 1993). Middle tropospheric heating anomalies (e.g., related to precipitation) can then affect the extratropical circulation by initiating Rossby wave trains in these waveguides (e.g., Simmons 1982; Hoskins and Ambrizzi 1993). Furthermore, quasi-stationary Rossby waves can be reflected by critical layers associated, for example, with zero-wind lines (Killworth and McIntyre 1985).

As found by Hoskins and Ambrizzi (1993), the background zonal flow is crucial for the propagation of Rossby waves. They found that the zonal stationary wavenumber K_s can be interpreted as a refractive index for Rossby waves and that regions with maxima in K_s act as waveguides. In spherical coordinates, K_s is given by

$$K_s = a\cos\phi\sqrt{\frac{\beta^*}{\overline{U}}}, \tag{1}$$

where $\overline{U}$ is a time mean of the upper-tropospheric zonal wind, ϕ is the latitude, a is the equatorial Earth radius, and

$$\beta^* = \frac{2\Omega\cos\phi}{a} - \frac{1}{a^2}\frac{\partial}{\partial\phi}\left[\frac{1}{\cos\phi}\frac{\partial}{\partial\phi}(\overline{U}\cos\phi)\right], \tag{2}$$

with Ω being Earth's rotation rate (see Barnes and Hartmann 2011). The zonal wavenumber K_s is then the number of zonal waves that would fit around the corresponding local latitude circle. We use full-field DJF monthly means of U200 as $\overline{U}$ here, representative of the upper troposphere. For $\overline{U}$ in Eqs. (1) and (2) we use composites of U200 averaged over months with $\widehat{[\mathrm{U150}]}_E$ greater than 1 (Fig. 8a) and less than −1 (Fig. 8b). Values are labeled as being significant when they exceed the 90% threshold, according to Monte Carlo simulations,[2] in fact

[2] To compute the significance levels Monte Carlo simulations are done. For this, 10 000 random time series X of the same length as $\widehat{[\mathrm{U150}]}_E$ from ERA-40 are drawn from a standard normal distribution. Subsequently, for each X the same procedure as for the observed time series of $\widehat{[\mathrm{U150}]}_E$ is applied to compute K_s; that is, U200 is averaged over months when X is greater than 1 or less than −1, respectively, and then K_s is computed using the average U200. For each of the two cases, the 5th and 95th percentiles of the distributions define the significance thresholds; in other words, they are the boundaries of the 90% range at each grid point.

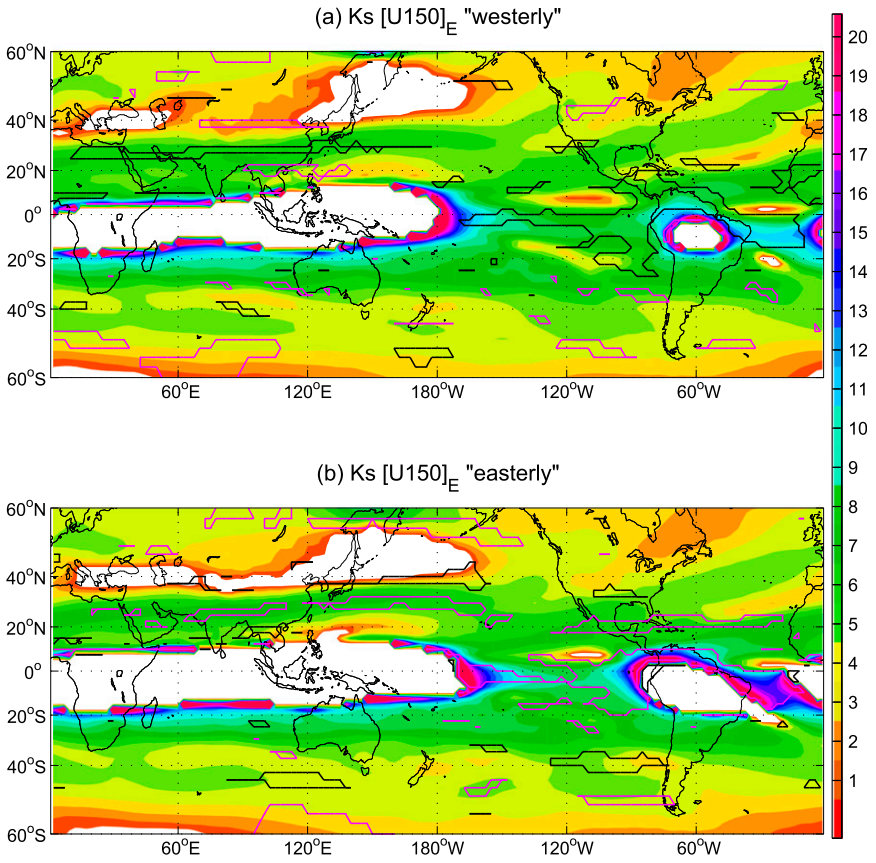

FIG. 8. The 200-hPa K_s, giving the number of waves that would fit around each corresponding latitude band (see color bar); K_s serves as a refractive index for the propagation of Rossby waves [see Eq. (1)]. (a) Value of K_s computed using U200 averaged over months from DJF when $\widehat{[U150]}_E$ is above 1. (b) As in (a), but for months from DJF when $\widehat{[U150]}_E$ is below −1. Black (magenta) contours indicate areas where the values are lower than (greater than) the 5th (95th) percentile of the probability distribution of 10 000 Monte Carlo simulations (see text for further information), in fact meaning that the values are significantly lower (black) or larger (magenta) than the climatology. White areas in (a) and (b) indicate nondefined values of K_s.

meaning that the values are significantly different from the climatology (see Hoskins and Ambrizzi 1993; Dawson et al. 2011).

The North Atlantic waveguide, originating in the eastern subtropical North Pacific, can be seen in both Figs. 8a and 8b and it is clear that it is on this waveguide that the North Atlantic wave train, noted when discussing Fig. 7, sits. There are also some differences in K_s between the westerly $\widehat{[U150]}_E$ and easterly $\widehat{[U150]}_E$ cases: First, in the tropics, K_s is larger in the easterly phase than in the westerly phase, especially over the eastern tropical Pacific and around South America, which is also the region where U200-EOF2 (see Fig. 4) has the largest amplitude. Notable also is the expansion (retraction) of the zero-wind line around the Amazon basin during the easterly (westerly) phase of $\widehat{[U150]}_E$. During the westerly phase, the subtropical waveguide over northern India and East Asia is slightly weaker and wider compared to the climatology. For the easterly phase of $\widehat{[U150]}_E$, the subtropical waveguides in the Northern Hemisphere are generally stronger, sharper, and more continuous. In particular, a stronger North Pacific waveguide during easterly $\widehat{[U150]}_E$ is consistent with the Z500 regression against $\widehat{[U150]}_E$, which indicates a southward shifted Aleutian low during the easterly phase (negative sign of the pattern shown in Figs. 7a,b). Farther downstream the connection between the North Pacific waveguide and the North Atlantic is stronger in the easterly phase and there is also a stronger connection between the North Atlantic and the tropical Atlantic–Africa waveguide during the easterly phase. The waveguide changes during easterly $\widehat{[U150]}_E$, providing a stronger link between the North Pacific and the North Atlantic, could be a part of the explanation for the wave train anomalies as found in the regression map of Z500 associated with $\widehat{[U150]}_E$ (Figs. 7a,b).

Honda et al. (2001) have investigated the connection between the Aleutian low and the Icelandic low by regressing late winter 250-hPa geopotential height onto their so-called seesaw index [see Figs. 6e,f in Honda et al. (2001)]. They find a pattern over the North Atlantic that is similar to the Z500 regression patterns associated with $\widehat{[U150]}_E$, shown in Figs. 7a and 7b, that is, the wave train over the North Atlantic that ends up with positive geopotential height anomalies over Europe. The change in the waveguide as shown in Fig. 8 associated with $\widehat{[U150]}_E$ could influence the seesaw relation between the Aleutian low and the Icelandic low as the easterly (westerly) phase of $\widehat{[U150]}_E$ favors (damps) the connection between the Pacific sector/Aleutian low and the North Atlantic sector/Icelandic low. We also note here that the climatological waveguide strengthens in February compared to December and January with a stronger link between the North Pacific and the North Atlantic in February (not shown here), possibly a reason why Honda et al. (2001) find the strongest link between the North Pacific and the North Atlantic during late winter.

To investigate the initiation of Rossby waves by anomalous divergent flow, we use the Rossby wave source (RWS), which is important in subtropical regions, where the divergent wind is strong and large horizontal gradients of absolute vorticity exist (Sardeshmukh and Hoskins 1988). The RWS is used here to identify the regions of effective tropical–extratropical influence associated with the $[U150]_E$ mode. As derived by Sardeshmukh and Hoskins (1988) from the nonlinear vorticity equation, the RWS is defined as

$$\mathrm{RWS} = -\mathbf{v}_\chi \cdot \nabla\zeta - \zeta\nabla \cdot \mathbf{v}_\chi, \tag{3}$$

where $\mathbf{v}_\chi$ is the divergent horizontal wind and $\zeta = f + \xi$ is the absolute vorticity, consisting of planetary vorticity f and relative vorticity ξ. Positive (negative) RWS anomalies then correspond to cyclonic (anticyclonic) vorticity forcing. The RWS is calculated at 200 hPa for both ERA-40 and the ensemble mean of the relaxation experiment CLIM-TROPICS and the regression onto the reference $\widehat{[U150]}_E$ index is shown in Fig. 9, together with the climatological RWS, calculated using ERA-40 data.

For ERA-40 data, the regression pattern associated with $\widehat{[U150]}_E$ is quite noisy, but some features stand out. The amplitude is about 3 times larger in the NH than in the Southern Hemisphere, if only the absolute maxima are considered. In the NH, associated with a positive $\widehat{[U150]}_E$ index, there is a band of positive RWS at about 30°N from northern India toward the North Pacific, negative RWS north of this band and over the eastern

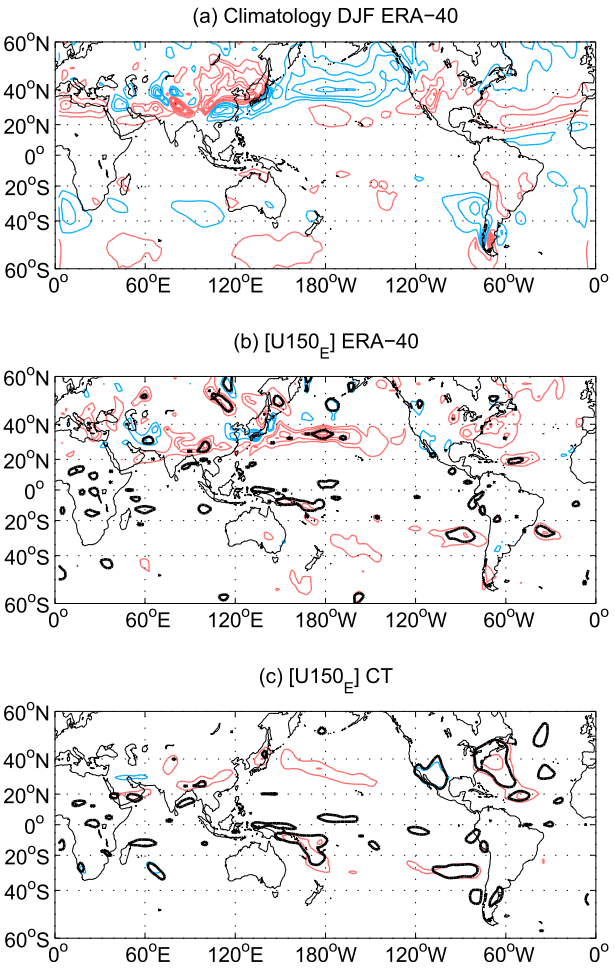

FIG. 9. Rossby wave source at 200 hPa (RWS200). (a) DJF climatology from ERA-40 data; (b) the linear regression pattern of RWS200 from ERA-40 onto the $\widehat{[U150]}_E$ index; (c) as in (b), but for RWS200 from the CLIM-TROPICS ensemble mean. Contour interval is $7.5 \times 10^{-11}\,\mathrm{s}^{-2}$ in (a) and $1.5 \times 10^{-11}\,\mathrm{s}^{-2}$ in (b) and (c), with red (blue) contours indicating positive (negative) anomalies, the zero lines being omitted. Black thick contours encircle areas where the correlation is significantly different from zero at the 95% level.

Pacific basin near North America, and positive RWS again over eastern North America and the adjacent North Atlantic. These features, except the band of negative RWS anomalies, are also visible in the plot for the ensemble mean of CLIM-TROPICS (Fig. 9c), albeit with reduced amplitude. The RWS anomalies over the central North Pacific are, however, no longer significant in the model and instead, the regression coefficients over North America are significant in the model. Overall, the regression pattern is less noisy for CLIM-TROPICS and in regions poleward of 50°N and 50°S the RWS regression is qualitatively zero in the ensemble mean, showing that the values in the regression for ERA-40 are probably noise there. The RWS anomalies near North America are

consistent with the wave train associated with $\widehat{[U150]}_E$ (Figs. 7a,b), since there are cyclonic (anticyclonic) anomalies downstream of the positive (negative) RWS anomalies. Anomalous RWS associated with the MJO was also noted by Cassou (2008, see his supplementary information), with a wavelike pattern in the region of the North Atlantic waveguide a few days after MJO phase 3, similar to the RWS regression presented in our Fig. 9, which we think is forced rather by late MJO phases. This author, however, considers only the first term on the right-hand side of Eq. (3) and looks at shorter time scales, which may limit the exact comparability of the results, but shows that the MJO has an impact on the North Atlantic sector.

The RWS anomalies presented in Fig. 9 are located precisely in the regions of the waveguides provided by the zonal-mean flow shown in Fig. 8. In particular, the North American RWS anomalies can initiate Rossby waves that propagate toward Europe via the North Atlantic waveguide and subsequently disturb the circulation there. This is true for both westerly and easterly phase of $\widehat{[U150]}_E$, but with a stronger link from the North Pacific to the North Atlantic and possibly stronger disturbance of the circulation over the North Atlantic in the case of easterly $\widehat{[U150]}_E$.

5. Application to the anomalous winter of 1962/63

The potential importance of the circulation mode associated with $[U150]_E$ is demonstrated by application to the winter of 1962/63 and compared with the role of the QBO. This winter was characterized by strong circulation anomalies over the whole NH and, in particular, extremely cold weather in northern Europe from the end of December until the end of February [see Greatbatch et al. (2014), who investigate the impacts of different factors: the tropical atmosphere, extratropical SST, and sea ice and the stratosphere on the circulation anomalies in the winter of 1962/63]. We shall concentrate on the DJF mean; that is, seasonal averages are taken both of the indices, $\widehat{[U150]}_E$ and QBO30, and of the Z500 data for the following analysis. It should be noted again that there is no correlation between the $\widehat{[U150]}_E$ and the QBO indices (see Table 1), enabling us to directly add the index-weighted regression patterns associated with the two indices separately. Let $R_p(x, y)$ be the regression of Z500 anomalies onto the $\widehat{[U150]}_E$ index and $Q_p(x, y)$ likewise for the QBO30 index, all for ERA-40 DJF mean data. Note that these regression coefficients are qualitatively, but not exactly, the same as those computed for monthly DJF data shown in Fig. 7. Then $R(x, y, t)$ and $Q(x, y, t)$ are the index-weighted regression patterns for each time step t (winter in this case):

$$R(x,\ y,\ t) = R_p(x,\ y)\widehat{[U150]}_E(t) \quad \text{and} \tag{4}$$

$$Q(x,\ y,\ t) = Q_p(x,\ y)\mathrm{QBO30}(t). \tag{5}$$

The DJF mean values of both indices in the particular winter of 1962/63 were extremely negative: $\widehat{[U150]}_E(1962/63) = -2.41$ and $\mathrm{QBO30}(1962/63) = -1.58$ (both indices are normalized to one standard deviation; see also the ERA-40 indices in Fig. 3). We also note here that the DJF mean $[U150]_E$ index has its absolute minimum in the ERA-40 record in the winter of 1962/63 [as noticed by Greatbatch et al. (2014)]. Shown in Fig. 10 is the Z500 anomaly of winter 1962/63 from ERA-40 in comparison with the linear combination $R(x, y, 1962/63) + Q(x, y, 1962/63)$ according to Eqs. (4) and (5) (hereafter, the indices x, y, and t are omitted for better readability). Also shown are the components R and Q for 1962/63 to clarify how they contribute to $R + Q$. Associated with $\widehat{[U150]}_E$ alone [$R(1962/63)$; Fig. 10b], we find very similar circulation anomalies compared to the reanalysis over the North Pacific sector and also over the polar regions. Over North America and the North Atlantic, $\widehat{[U150]}_E$ is associated with the wave train pattern discussed above, which is similar to the anomalies in the reanalysis in 1962/63, especially in January 1963 (Greatbatch et al. 2014, see their Fig. 6). The only deficit occurs over western Europe, where the anomaly in $R(1962/63)$ is slightly more zonally oriented than in ERA-40. As noted before, the wave train is clearer in the CLIMTROPICS experiment (see Fig. 7b), but using CLIMTROPICS does not improve the result over Europe, as the anomalies are slightly shifted compared to the reanalysis. It is of interest to note that during winter 1962/63, the MJO was suppressed (not shown), consistent with the easterly anomaly in $\widehat{[U150]}_E$ that winter (see Fig. 5), which, interestingly, began shortly before the onset of the severe weather in Europe and ended with the breakdown of the severe weather in Europe (see Fig. 2b in Greatbatch et al. 2014).

The influence of the QBO in this winter (Fig. 10c) has a signature over the North Atlantic that is very similar to the negative NAO pattern and therefore contributes to a more meridional dipole there that gives some extra skill to the combination $R + Q$. According to the Holton and Tan (1980) mechanism, it is possible that the easterly phase of the QBO in 1962/63 favored the stratospheric warming that occurred in late January 1963, which in turn impacted the troposphere [see Greatbatch et al. (2014), their Figs. 7 and 11]. The combination $R + Q$ (Fig. 10d) thus results in an anomaly pattern qualitatively very similar to the reanalysis anomaly over the whole NH extratropics. This suggests that the extreme

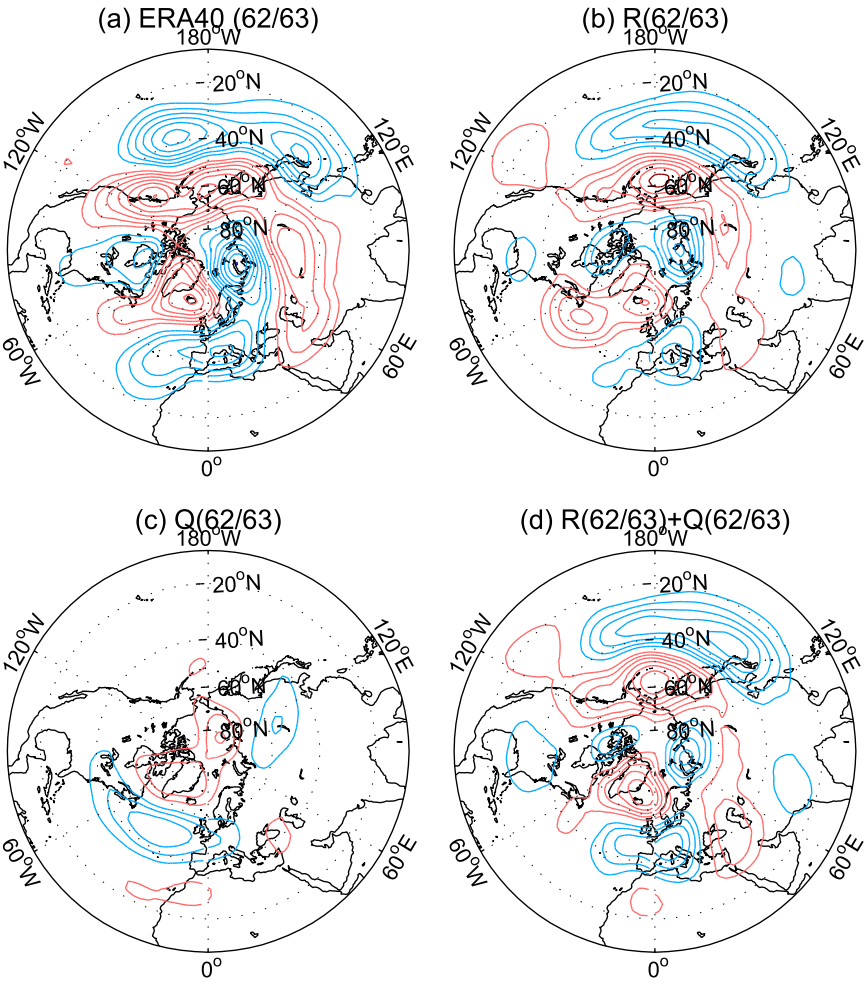

FIG. 10. The Z500 DJF mean anomalies for winter 1962/63. (a) The ERA-40 anomaly with respect to the climatological winter mean from 1960/61 to 2001/02, and (b) the component $R(x, y, 1962/63)$ and (c) the component $Q(x, y, 1962/63)$ according to Eqs. (4) and (5), respectively. (d) The linear combination $R(x, y, 1962/63) + Q(x, y, 1962/63)$. Contour intervals are 16 m for (a) and 8 m for (b)–(d), with red (blue) contours indicating positive (negative) anomalies and the zero lines being omitted.

negative value of $\widehat{[U150]}_E$ was a significant factor in the dynamics of this severely cold European winter with some additional influence of the QBO. However, $R + Q$ can only explain half of the amplitude of the observed anomaly. The rest of the amplitude may be caused by internal variability (e.g., eddy mean–flow feedback) or other influences we have not considered here (see Folland et al. 2012; Greatbatch et al. 2014). We also note here that during winters when $\widehat{[U150]}_E$ and lower stratospheric QBO have the opposite sign (see Fig. 3), patterns $R(t)$ and $Q(t)$ tend to cancel each other out over the North Atlantic and Europe. Furthermore, winters with $\widehat{[U150]}_E$/QBO30 indices of the same sign and strong amplitude do not occur very often during the period 1949–2013 covered by the reanalysis datasets. In fact, the only candidate for a comparable test is 1983/84, when both $\widehat{[U150]}_E$ and QBO30 were strongly negative, and the Z500 anomalies of 1983/84 (not shown) reveal anomalies over the North Pacific and North America which are similar to the regression onto $\widehat{[U150]}_E$. The beginning of a wave train toward Europe is also visible, but it is then overwhelmed by geopotential anomalies projecting onto the positive NAO pattern. Indeed, this winter was characterized by a positive NAO index and only very weak surface temperature anomalies over Europe, indicating that other factors can sometimes dominate the winter climate over Europe. In the case of 1983/84, a possible additional influence would be the residual effect of the strong 1982/83 El Niño event.

6. Summary and discussion

Updating the rotated EOF analysis of Nigam (1990) applied to DJF monthly-mean zonal-mean zonal wind ($[U]$) anomalies at all latitudes, we find four dominant modes in the reanalysis datasets NCEP–NCAR, ERA-40, and ERA-Interim. Three of the four modes correspond to widely known circulation modes of the atmosphere: The first two modes are the NAM and SAM, explaining most of the variance of $[U]$ in the extratropics of their respective hemispheres. Modes 3 and 4 are confined to the tropics and, while noting that both explain slightly more than 20% of the variance of tropical $[U]$, both can be associated with physically distinct mechanisms. One of the two is closely related to ENSO and is therefore, as for the first two modes, not investigated in detail in the present paper. Indeed, it is the mode that describes the equatorial upper-tropospheric $[U]$, which has been investigated in detail here by using the time series of monthly anomalies of $[U]$ at 150 hPa averaged between 5°S and 5°N $[\mathrm{U150}]_E$, as this time series is highly correlated with the principal component time series of the REOF mode. The $[\mathrm{U150}]_E$ mode was shown to be related to the MJO, since the propagating diabatic heating anomalies of the MJO favor upper-tropospheric westerly (easterly) anomalies, especially in late (early) MJO phases. Furthermore, the absence (presence) of MJO activity has been shown to favor easterly (westerly) $[\mathrm{U150}]_E$ anomalies, consistent with previous studies (e.g., Hoskins et al. 1999; Kraucunas and Hartmann 2005).

Long-term trends and low-frequency variability of $[\mathrm{U150}]_E$ are not discussed in the present paper, as all data have been detrended prior to the analysis and we focus on the seasonal to interannual time scales. Interestingly though, we note here a correlation, albeit weak, of $r = 0.22$ between $[\mathrm{U150}]_E$ and the normalized time series of sunspot activity (as downloaded from http://www.esrl.noaa.gov/psd/gcos_wgsp/Timeseries/Data/sunspot.long.data, an estimate of variations in total solar incoming radiation, mainly representing the 11-yr solar cycle). This is consistent with the observational results of Haigh et al. (2005, see their Fig. 1c), who use a different measure for solar activity (i.e., the 10.7-cm flux) and perform a multiple linear regression on $[U]$, but do not discuss the equatorial signal in their results. A possible explanation for the positive correlation is that during solar maxima, the mean meridional overturning circulation is weaker and therefore can remove less westerly momentum from the equatorial upper troposphere (Kraucunas and Hartmann 2005). Indeed, given that anomalies of $[\mathrm{U150}]_E$ can impact the North Atlantic sector (see Figs. 7 and 10), this mechanism could be another pathway for the connection between solar activity and European winter weather that has been noted by previous studies (e.g., by Lockwood et al. 2010). These authors noted that periods of low solar activity go along with periods of more frequent Atlantic blockings and hence more severe winter weather in Europe, of which 1962/63 (at the time of a solar minimum) is a striking example. We also note here that the undetrended time series of $[\mathrm{U150}]_E$ has a strong trend toward westerly values (between $+0.27$ and $+0.46\,\mathrm{m\,s^{-1}\,decade^{-1}}$ in the different reanalyses). However, Allen and Sherwood (2008) find exactly the opposite trend in tropical upper-tropospheric $[U]$ by using direct radiosonde measurements, which points to possible inconsistencies in the reanalyses regarding long-term trends in this region.

The second part of the paper focuses on the extratropical influence of $[\mathrm{U150}]_E$ on monthly-to-seasonal time scales. We make use of an experiment with the ECMWF model, in which the tropical atmosphere has been relaxed toward ERA-40 data, which is why we focus on this reanalysis dataset in this part of the study. We use linear regression onto the time series $\widehat{[\mathrm{U150}]}_E$ (linear influence of ENSO, as measured by Niño-3.4, removed and normalized to one standard deviation) of Z500 data from both the ERA-40 reanalysis and the ensemble mean from the relaxation experiment (CLIM-TROPICS) and also compare with a corresponding regression onto the QBO index defined at 30 hPa.

While the positive QBO index is associated with a positive NAO pattern, consistent with many other studies, the westerly phase of $\widehat{[\mathrm{U150}]}_E$ is associated with a northward shift of the Aleutian low in both reanalysis and model results. In addition to the anomalies over the North Pacific, we identify a wave train from the southwest of North America toward Europe. This wave train becomes much clearer in the model results, where the wave train is of stronger amplitude than the signal over the western North Pacific.

Analysis of the zonal stationary wavenumber diagnostic (K_s; Hoskins and Ambrizzi 1993; Barnes and Hartmann 2011) reveals a stronger than normal waveguide especially over the North Pacific during the easterly phase of $[\mathrm{U150}]_E$ with a slightly stronger link to the North Atlantic and also the hint of a link between the extratropical and tropical Atlantic waveguides. The former change suggests a role of the equatorial upper-tropospheric winds for explaining the "seesaw" between the Aleutian low and the Icelandic low as noted by Honda et al. (2001). Rossby wave source (RWS; Sardeshmukh and Hoskins 1988) anomalies associated with $[\mathrm{U150}]_E$ were found to be strongest and most robust in the linking region of the North Pacific and the North Atlantic waveguide, and are probably associated with the Rossby wave train over the North Atlantic as found in the regression of Z500 against $\widehat{[\mathrm{U150}]}_E$, especially in the model.

Over the western North Pacific, $[U150]_E$ has been found to be important for the winter circulation, and can therefore be useful for statistical seasonal prediction. It might be that the signal associated with $[U150]_E$ is relatively weak over the North Atlantic and Europe compared to other influences, as can be seen when comparing the winters of 1962/63 and 1983/84, both of which were associated with an extremely easterly phase of $[U150]_E$ and the easterly phase of the QBO. The differences in detail of the regression patterns shown in Figs. 7a,b also suggest that the impact of $[U150]_E$ is not strong over Europe, although in certain winters (e.g., 1962/63) the impact could be important. Indeed, the circulation anomalies of winter 1962/63 agree well with the combined influence from both $[U150]_E$ and the QBO over large parts of the NH, including the European sector, while those of 1983/84 (when $\widetilde{[U150]}_E$ and QBO30 had similar values as in 1962/63) only agree well over the Pacific sector and are dominated by a positive NAO signal over the North Atlantic. This in turn might have been a residual effect of the strong El Niño event in 1983. We noted, nevertheless, that the decorrelation time scale for $[U150]_E$ anomalies is several months (see Fig. 2) and this, combined with the good performance in 1962/63, suggests that $[U150]_E$ could be important for seasonal and medium-range prediction.

Acknowledgments. We want to thank the ECMWF for the provision of the model data and especially Prof. Dr. Thomas Jung and Dr. Soumia Serrar who carried out the model runs reported here. We also thank Dr. Lisa Neef and Dr. Remi Thieblemont from GEOMAR for discussions that drew our attention to the tropospheric $[U]$ along the equator and Prof. Adrian Matthews, who made very useful suggestions about the K_s diagnostic. Additionally, we thank three anonymous reviewers for helpful comments that led to a substantial improvement of this manuscript. GG has been funded by the DFG under ISOLAA, a project within the Priority Programme 1158, and RJG has been supported by GEOMAR, Kiel.

REFERENCES

Allen, R. J., and S. C. Sherwood, 2008: Warming maximum in the tropical upper troposphere deduced from thermal winds. *Nat. Geosci.,* **1,** 399–403, doi:10.1038/ngeo208.

Baldwin, M. P., and T. J. Dunkerton, 2001: Stratospheric harbingers of anomalous weather regimes. *Science,* **294,** 581–584, doi:10.1126/science.1063315.

——, and Coauthors, 2001: The quasi-biennial oscillation. *Rev. Geophys.,* **39,** 179–229, doi:10.1029/1999RG000073.

Barnes, E. A., and D. L. Hartmann, 2011: Rossby wave scales, propagation, and the variability of eddy-driven jets. *J. Atmos. Sci.,* **68,** 2893–2908, doi:10.1175/JAS-D-11-039.1.

Barnston, A., and R. Livezey, 1987: Classification, seasonality, and persistence of low-frequency atmospheric circulation patterns. *Mon. Wea. Rev.,* **115,** 1083–1126, doi:10.1175/1520-0493(1987)115<1083:CSAPOL>2.0.CO;2.

Boer, G. J., and K. Hamilton, 2008: QBO influence on extratropical predictive skill. *Climate Dyn.,* **31,** 987–1000, doi:10.1007/s00382-008-0379-5.

Cassou, C., 2008: Intraseasonal interaction between the Madden–Julian oscillation and the North Atlantic Oscillation. *Nature,* **455,** 523–527, doi:10.1038/nature07286.

Dawson, A., A. J. Matthews, and D. P. Stevens, 2011: Rossby wave dynamics of the North Pacific extra-tropical response to El Niño: Importance of the basic state in coupled GCMs. *Climate Dyn.,* **37,** 391–405, doi:10.1007/s00382-010-0854-7.

Dee, D. P., and Coauthors, 2011: The ERA-Interim reanalysis: Configuration and performance of the data assimilation system. *Quart. J. Roy. Meteor. Soc.,* **137,** 553–597, doi:10.1002/qj.828.

Ding, H., R. J. Greatbatch, and G. Gollan, 2014a: Tropical influence independent of ENSO on the austral summer southern annular mode. *Geophys. Res. Lett.,* **41,** 3643–3648, doi:10.1002/2014GL059987.

——, ——, and ——, 2014b: Tropical impact on the interannual variability and long-term trend of the southern annular mode during austral summer from 1960/1961 to 2001/2002. *Climate Dyn.,* doi:10.1007/s00382-014-2299-x, in press.

——, ——, W. Park, M. Latif, V. A. Semenov, and X. Sun, 2014c: The variability of the East Asian summer monsoon and its relationship to ENSO in a partially coupled climate model. *Climate Dyn.,* **42,** 367–379, doi:10.1007/s00382-012-1642-3.

Ding, Q., E. J. Steig, D. S. Battisti, and J. M. Wallace, 2012: Influence of the tropics on the southern annular mode. *J. Climate,* **25,** 6330–6348, doi:10.1175/JCLI-D-11-00523.1.

Ding, R., J. Li, and K.-H. Seo, 2010: Predictability of the Madden–Julian oscillation estimated using observational data. *Mon. Wea. Rev.,* **138,** 1004–1013, doi:10.1175/2009MWR3082.1.

Dommenget, D., and M. Latif, 2002: A cautionary note on the interpretation of EOFs. *J. Climate,* **15,** 216–225, doi:10.1175/1520-0442(2002)015<0216:ACNOTI>2.0.CO;2.

Folland, C. K., A. A. Scaife, J. Lindesay, and D. B. Stephenson, 2012: How potentially predictable is northern European winter climate a season ahead? *Int. J. Climatol.,* **32,** 801–818, doi:10.1002/joc.2314.

Gollan, G., R. J. Greatbatch, and T. Jung, 2012: Tropical impact on the East Asian winter monsoon. *Geophys. Res. Lett.,* **39,** L17801, doi:10.1029/2012GL052978.

Greatbatch, R. J., 2000: The North Atlantic Oscillation. *Stochastic Environ. Res. Risk Assess.,* **14,** 213–242, doi:10.1007/s004770000047.

——, H. Lin, J. Lu, K. A. Peterson, and J. Derome, 2003: Tropical/extratropical forcing of the AO/NAO: A corrigendum. *Geophys. Res. Lett.,* **30,** 1738, doi:10.1029/2003GL017406.

——, J. Lu, and K. A. Peterson, 2004: Nonstationary impact of ENSO on Euro-Atlantic winter climate. *Geophys. Res. Lett.,* **31,** L02208, doi:10.1029/2003GL018542.

——, G. Gollan, T. Jung, and T. Kunz, 2012a: Factors influencing Northern Hemisphere winter mean atmospheric circulation anomalies during the period 1960/61 to 2001/02. *Quart. J. Roy. Meteor. Soc.,* **138,** 1970–1982, doi:10.1002/qj.1947.

——, ——, and ——, 2012b: An analysis of trends in the boreal winter mean tropospheric circulation during the second half of the 20th century. *Geophys. Res. Lett.,* **39,** L13809, doi:10.1029/2012GL052243.

——, ——, ——, and T. Kunz, 2014: Tropical origin of the severe European winter of 1962/63. *Quart. J. Roy. Meteor. Soc.,* doi:10.1002/qj.2346, in press.

Haigh, J. D., M. Blackburn, and R. Day, 2005: The response of tropospheric circulation to perturbations in lower-stratospheric temperature. *J. Climate,* **18,** 3672–3685, doi:10.1175/JCLI3472.1.

Held, I. M., and A. Y. Hou, 1980: Nonlinear axially symmetric circulations in a nearly inviscid atmosphere. *J. Atmos. Sci.,* **37,** 515–533, doi:10.1175/1520-0469(1980)037<0515:NASCIA>2.0.CO;2.

Hoerling, M. P., J. W. Hurrell, and T. Xu, 2001: Tropical origins for recent North Atlantic climate change. *Science,* **292,** 90–92, doi:10.1126/science.1058582.

Holton, J. R., and H.-C. Tan, 1980: The influence of the equatorial quasi-biennial oscillation on the global circulation at 50 mb. *J. Atmos. Sci.,* **37,** 2200–2208, doi:10.1175/1520-0469(1980)037<2200:TIOTEQ>2.0.CO;2.

Honda, M., H. Nakamura, J. Ukita, I. Kousaka, and K. Takeuchi, 2001: Interannual seesaw between the Aleutian and Icelandic lows. Part I: Seasonal dependence and life cycle. *J. Climate,* **14,** 1029–1042, doi:10.1175/1520-0442(2001)014<1029:ISBTAA>2.0.CO;2.

Hoskins, B. J., and T. Ambrizzi, 1993: Rossby wave propagation on a realistic longitudinally varying flow. *J. Atmos. Sci.,* **50,** 1661–1671, doi:10.1175/1520-0469(1993)050<1661:RWPOAR>2.0.CO;2.

——, R. Neale, M. Rodwell, and G.-Y. Yang, 1999: Aspects of the large-scale tropical atmospheric circulation. *Tellus,* **51B,** 33–44, doi:10.1034/j.1600-0889.1999.00004.x.

Hurrell, J. W., Y. Kushnir, G. Ottersen, and M. Visbeck, 2003: An overview of the North Atlantic oscillation. *The North Atlantic Oscillation: Climatic Significance and Environmental Impact, Geophys. Monogr.,* Vol. 134, Amer. Geophys. Union, 1–36.

Ineson, S., and A. A. Scaife, 2009: The role of the stratosphere in the European climate response to El Niño. *Nat. Geosci.,* **2,** 32–36, doi:10.1038/ngeo381.

Jung, T., T. N. Palmer, M. J. Rodwell, and S. Serrar, 2010a: Understanding the anomalously cold European winter of 2005/06 using relaxation experiments. *Mon. Wea. Rev.,* **138,** 3157–3174, doi:10.1175/2010MWR3258.1.

——, and Coauthors, 2010b: The ECMWF model climate: Recent progress through improved physical parametrizations. *Quart. J. Roy. Meteor. Soc.,* **136,** 1145–1160, doi:10.1002/qj.634.

Kalnay, E., and Coauthors, 1996: The NCEP/NCAR 40-Year Reanalysis Project. *Bull. Amer. Meteor. Soc.,* **77,** 437–471, doi:10.1175/1520-0477(1996)077<0437:TNYRP>2.0.CO;2.

Killworth, P. D., and M. E. McIntyre, 1985: Do Rossby-wave critical layers absorb, reflect, or over-reflect? *J. Fluid Mech.,* **161,** 449–492, doi:10.1017/S0022112085003019.

Kraucunas, I., and D. L. Hartmann, 2005: Equatorial superrotation and the factors controlling the zonal-mean zonal winds in the tropical upper troposphere. *J. Atmos. Sci.,* **62,** 371–389, doi:10.1175/JAS-3365.1.

Lee, S., 1999: Why are the climatological zonal winds easterly in the equatorial upper troposphere? *J. Atmos. Sci.,* **56,** 1353–1363, doi:10.1175/1520-0469(1999)056<1353:WATCZW>2.0.CO;2.

L'Heureux, M. L., and D. W. J. Thompson, 2006: Observed relationships between the El Niño–Southern Oscillation and the extratropical zonal-mean circulation. *J. Climate,* **19,** 276–287, doi:10.1175/JCLI3617.1.

Lin, H., G. Brunet, and J. Derome, 2009: An observed connection between the North Atlantic Oscillation and the Madden–Julian oscillation. *J. Climate,* **22,** 364–380, doi:10.1175/2008JCLI2515.1.

Lockwood, M., R. G. Harrison, T. Woollings, and S. K. Solanki, 2010: Are cold winters in Europe associated with low solar activity? *Environ. Res. Lett.,* **5,** 024001, doi:10.1088/1748-9326/5/2/024001.

Lu, H., T. J. Bracegirdle, T. Phillips, A. Bushell, and L. Gray, 2014: Mechanisms for the Holton–Tan relationship and its decadal variation. *J. Geophys. Res. Atmos.,* **119,** 2811–2830, doi:10.1002/2013JD021352.

Marshall, A. G., and A. A. Scaife, 2009: Impact of the QBO on surface winter climate. *J. Geophys. Res.,* **114,** D18110, doi:10.1029/2009JD011737.

Moore, G. W. K., and I. A. Renfrew, 2012: Cold European winters: Interplay between the NAO and the East Atlantic mode. *Atmos. Sci. Lett.,* **13,** 1–8, doi:10.1002/asl.356.

Nigam, S., 1990: On the structure of variability of the observed tropospheric and stratospheric zonal-mean zonal wind. *J. Atmos. Sci.,* **47,** 1799–1813, doi:10.1175/1520-0469(1990)047<1799:OTSOVO>2.0.CO;2.

Oort, A. H., and J. J. Yienger, 1996: Observed interannual variability in the Hadley circulation and its connection to ENSO. *J. Climate,* **9,** 2751–2767, doi:10.1175/1520-0442(1996)009<2751:OIVITH>2.0.CO;2.

Sardeshmukh, P. D., and B. J. Hoskins, 1988: The generation of global rotational flow by steady idealized tropical divergence. *J. Atmos. Sci.,* **45,** 1228–1251, doi:10.1175/1520-0469(1988)045<1228:TGOGRF>2.0.CO;2.

Seager, R., N. Harnik, Y. Kushnir, W. Robinson, and J. Miller, 2003: Mechanisms of hemispherically symmetric climate variability. *J. Climate,* **16,** 2960–2978, doi:10.1175/1520-0442(2003)016<2960:MOHSCV>2.0.CO;2.

Simmons, A. J., 1982: The forcing of stationary wave motion by tropical diabatic heating. *Quart. J. Roy. Meteor. Soc.,* **108,** 503–534, doi:10.1002/qj.49710845703.

Slingo, J. M., and Coauthors, 1996: Intraseasonal oscillations in 15 atmospheric general circulation models: Results from an AMIP diagnostic subproject. *Climate Dyn.,* **12,** 325–357, doi:10.1007/BF00231106.

Sun, X., R. J. Greatbatch, W. Park, and M. Latif, 2010: Two major modes of variability of the East Asian summer monsoon. *Quart. J. Roy. Meteor. Soc.,* **136,** 829–841, doi:10.1002/qj.635.

Thompson, D. W. J., and J. M. Wallace, 2000: Annular modes in the extratropical circulation. Part I: Month-to-month variability. *J. Climate,* **13,** 1000–1016, doi:10.1175/1520-0442(2000)013<1000:AMITEC>2.0.CO;2.

Trenberth, K. E., G. W. Branstator, D. Karoly, A. Kumar, N.-C. Lau, and C. Ropelewski, 1998: Progress during TOGA in understanding and modeling global teleconnections associated with tropical sea surface temperatures. *J. Geophys. Res.,* **103,** 14 291–14 324, doi:10.1029/97JC01444.

Uppala, S. M., and Coauthors, 2005: The ERA-40 Re-Analysis. *Quart. J. Roy. Meteor. Soc.,* **131,** 2961–3012, doi:10.1256/qj.04.176.

von Storch, H., and F. W. Zwiers, 2001: *Statistical Analysis in Climate Research.* Cambridge University Press, 484 pp.

Walker, G., and E. Bliss, 1932: World weather V. *Mem. Roy. Meteor. Soc.,* **4** (36), 53–84.

Wang, L., W. Chen, and R. Huang, 2008: Interdecadal modulation of PDO on the impact of ENSO on the East Asian winter monsoon. *Geophys. Res. Lett.,* **35,** L20702, doi:10.1029/2008GL035287.

Wheeler, M. C., and H. H. Hendon, 2004: An all-season real-time multivariate MJO index: Development of an index for monitoring and prediction. *Mon. Wea. Rev.,* **132,** 1917–1932, doi:10.1175/1520-0493(2004)132<1917:AARMMI>2.0.CO;2.